
TPS-Drive: Task-Guided Representation Purification for VLM-based Autonomous Driving

Jiayang Li¹, Yumao Liu¹, Ke Ma^{1*}

¹The Hong Kong University of Science and Technology (Guangzhou), Guangzhou, China
zmbdsilver@gmail.com, yliu313@hkust-gz.edu.cn, kema@hkust-gz.edu.cn

Abstract

Vision-Language Models (VLMs) provide a promising foundation for autonomous driving planning, yet bridging semantic reasoning and precise 3D spatial forecasting remains a critical challenge. Existing representation strategies generally follow two paths: text-aligned methods flatten continuous spatial states into symbols, which compromises geometric structure and induces "spatial hallucinations"; dense visual methods preserve spatial topology but overwhelm standard tokenizers with redundant background textures, leading to "representation interference". To address these limitations, we introduce TPS-Drive, a novel framework centered on Task-Guided Representation Purification that empowers VLMs to *Think in Purified Space*. At its core, an Agent-Centric Tokenizer utilizes a task-guided vector quantization mechanism supervised by a frozen 3D detection head, which explicitly reallocates limited codebook capacity from pervasive static backgrounds to critical dynamic agents and effectively isolates spatial redundancy. Leveraging this purified spatial vocabulary, TPS-Drive employs a decoupled reasoning pipeline that sequentially performs scene understanding, future forecasting, and action generation. The framework is optimized via a progressive three-stage training paradigm, culminating in reward-driven refinement that surpasses pure imitation learning. Extensive experiments validate our approach: TPS-Drive achieves accurate agent spatial state forecasting and reduces collision rates in open-loop nuScenes evaluations, while establishing new safety records on the rigorous closed-loop NAVSIMv1 and NAVSIMv2 benchmarks.

1 Introduction

Vision-Language Models (VLMs) provide a promising foundation for autonomous driving planning through strong semantic reasoning on multimodal inputs[1, 2, 3]. However, their language-centric architectures are not naturally designed to model continuous geometric structures[4] and temporal dynamics[5]. This limitation becomes critical in autonomous driving, where executable actions require accurate forecasting of agent spatial state evolution in 3D physical space[6]. Thus, designing a representation that bridges the gap between semantic reasoning and precise forecasting of agent spatial states remains a key challenge for VLM-based autonomous driving systems.

Existing methods typically address this challenge through two primary representation strategies, as illustrated in Figure 1. The first strategy relies on text[7, 8] or numerical[9] formats (Figure 1A), representing spatial states through either natural language descriptions (e.g., *ahead, right*) or flattened 3D box coordinates. While such text-aligned representations integrate seamlessly with standard VLM tokenizers, mapping continuous spatial states to discrete symbols compromises the underlying geometric structure of physical space[10]. Thus, this geometry-agnostic discretization often induces

*Corresponding author

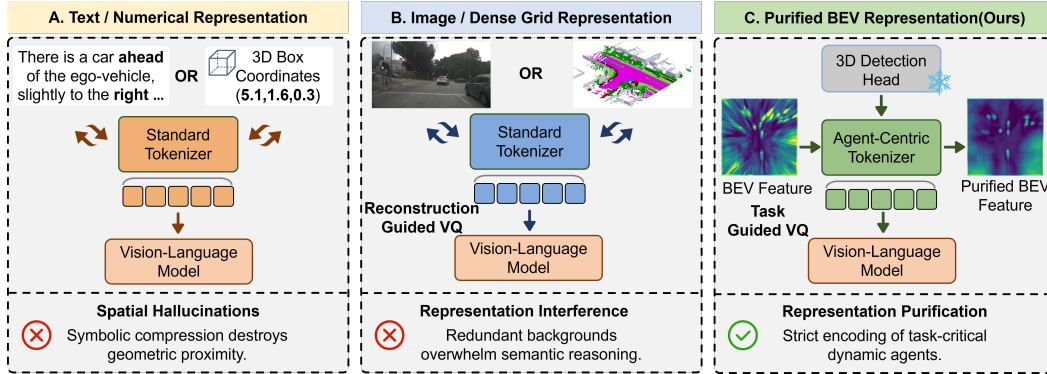


Figure 1: **Comparison of representation strategies.** (A) Text and numerical formats induce spatial hallucinations, as symbolic compression destroys geometric proximity. (B) Dense grid representations cause representation interference, where redundant backgrounds overwhelm semantic reasoning. (C) Our **TPS-Drive** achieves representation purification via task-guided VQ, enabling the strict encoding of task-critical dynamic agents.

"spatial hallucinations" and limits the VLM's ability to precisely capture the continuous spatial states of dynamic agents.

The second strategy employs image or dense grid representations (Figure 1B), such as forecasting future images overlaid with 3D boxes[11] or modeling dense 3D occupancy grids[12]. Compared with text-based representations, dense representations better preserve spatial topology. However, they also contain large regions of repetitive or weakly task-relevant content, such as static backgrounds and texture details. Driven by reconstruction-guided Vector Quantization (VQ)[13], standard tokenizers in this paradigm treat all dense features equally. They disproportionately allocate their limited codebook capacity to static background and redundant textures rather than to critical dynamic agents. Thus, feeding these spatial tokens into the VLM induces severe "representation interference" that overwhelms the model's semantic reasoning capabilities.

To overcome these limitations, we introduce TPS-Drive—a framework centered on task-guided representation purification that enables the VLM to *Think in Purified Space*. Rather than flattening continuous 3D coordinates or burdening the model with redundant dense inputs, TPS-Drive constructs an agent-centric, purified Bird's-Eye-View (BEV) representation (Figure 1C). At its core, an Agent-Centric Tokenizer employs a task-guided VQ mechanism supervised by a frozen 3D detection head. This design explicitly reallocates limited codebook capacity from static background and redundant textures to critical dynamic agents. This "representation purification" effectively isolates spatial redundancy from semantic reasoning, empowering the VLM to ingest purified 3D tokens.

Equipped with this purified spatial vocabulary, TPS-Drive executes a decoupled reasoning pipeline: it first extracts static environmental context and physical rules, then forecasts the spatial state evolution of dynamic agents, and ultimately generates continuous ego trajectories. This pipeline is optimized via a progressive three-stage training paradigm. The process begins with task-guided pretraining for the agent-centric tokenizer. The VLM is then optimized via Supervised Fine-Tuning (SFT) to jointly master scene understanding, future forecasting, and action generation. Ultimately, reward-driven refinement further aligns the final policy with safety-oriented objectives.

Extensive experiments on nuScenes, NAVSIMv1, and NAVSIMv2 validate the effectiveness of TPS-Drive. On nuScenes, TPS-Drive improves agent-centric spatial forecasting and achieves strong collision-avoidance performance in open-loop planning. In closed-loop settings, it delivers robust planning performance on NAVSIMv1 and establishes new safety records under the rigorous interactive pseudo-simulation of NAVSIMv2. The main contributions are as follows:

- We propose an Agent-Centric Tokenizer supervised by a frozen 3D detection head. This achieves task-guided representation purification by explicitly isolating spatial redundancy, empowering the VLM to *Think in Purified Space*.

- We introduce TPS-Drive, a decoupled framework for scene understanding, future forecasting, and action generation, optimized via a three-stage training paradigm featuring reward-driven refinement that surpasses pure imitation learning.
- TPS-Drive achieves exceptional spatial forecasting and minimal collision rates on open-loop nuScenes, while establishing new safety records on the rigorous closed-loop NAVSIMv1 and NAVSIMv2 benchmarks.

2 Related Work

2.1 Vision-Language Models in Autonomous Driving

Recent advances in multimodal learning[14, 15] have spurred the development of VLMs for end-to-end autonomous driving[16, 17]. Within this domain, researchers are increasingly adapting these architectures to process complex traffic scenarios[18, 19, 20]. For instance, DriveGPT4[21] uses a video-based VLM for textual explanations and control. LMDrive[22] processes multimodal inputs alongside language instructions to output closed-loop waypoints[23, 24, 25]. Additionally, DriveMLM[26] compresses sensor data via a multimodal tokenizer for behavioral planning alignment. To improve spatial reasoning, OmniDrive[27] explicitly aligns 3D perception features with language models. Expanding on this, BEVDriver[28] and OccVLA[29] fuse dense Bird’s-Eye-View or occupancy representations directly into the VLM’s token space. While these models demonstrate impressive capabilities, they fundamentally face a trade-off between geometric fidelity and computational efficiency[30], often leading to spatial hallucinations[31, 32] or representation interference[33]. Unlike these approaches, our proposed TPS-Drive introduces a task-guided mechanism to purify spatial features prior to VLM reasoning.

2.2 World Models for Spatial Forecasting

World models[34, 35, 36] play a critical role in anticipating the spatial state evolution of dynamic agents for safe autonomous planning. Existing methods[37, 38] typically follow two distinct trajectories. The first leverages dense continuous representations, such as predicting future Bird’s-Eye-View maps[39], point clouds[40, 41], or occupancy grids[12, 42]. OccWorld [12] and DriveWorld [43] forecast continuous 3D occupancy volumes to successfully preserve geometric structures. Conversely, driven by the scalability of large language models[44, 45], the second trajectory employs discrete tokenization. Frameworks like GAIA-1 [46], MILE [47], and recent generative world models[48, 49] utilize reconstruction-guided Vector Quantization[50] to discretize scenes for autoregressive prediction. However, these standard tokenizers are inherently burdened by representation redundancy[51], misallocating codebook capacity to massive static backgrounds. To overcome this limitation, TPS-Drive explicitly isolates this spatial redundancy, shifting from global reconstruction to task-guided purification to yield highly distilled 3D tokens focused entirely on dynamic agents.

2.3 Spatial Representation and Scene Tokenization

3D spatial representation[52] in VLMs typically follows text-based serialization[53, 54] or dense representation paradigms[55, 56]. Text-based methods like LMDrive[22] and Drivegpt4[21] discretize 3D coordinates into numerical tokens, which often compromises the underlying geometric structure. Conversely, dense tokenizers like VQ-VAE[57] rely on reconstruction objectives that overwhelm the codebook with redundant background textures. To address this, OccLLaMA[58] discretizes semantic occupancy to explicitly handle spatial sparsity. Furthering this trend, TPS-Drive employs an agent-centric tokenizer to yield distilled 3D tokens focused exclusively on dynamic agents, empowering the model to think in purified space.

3 Method

3.1 Preliminary

As illustrated in Figure 2, TPS-Drive formulates autonomous driving as a decoupled three-stage reasoning process. At time t , the ego-vehicle processes multi-view images $\mathcal{I}_t = \{\mathcal{I}_t^c\}_{c=1}^C$ from C surrounding cameras and an ego-centric Bird’s-Eye-View (BEV) feature map $\mathcal{B}_t \in \mathbb{R}^{D \times H \times W}$ [59],

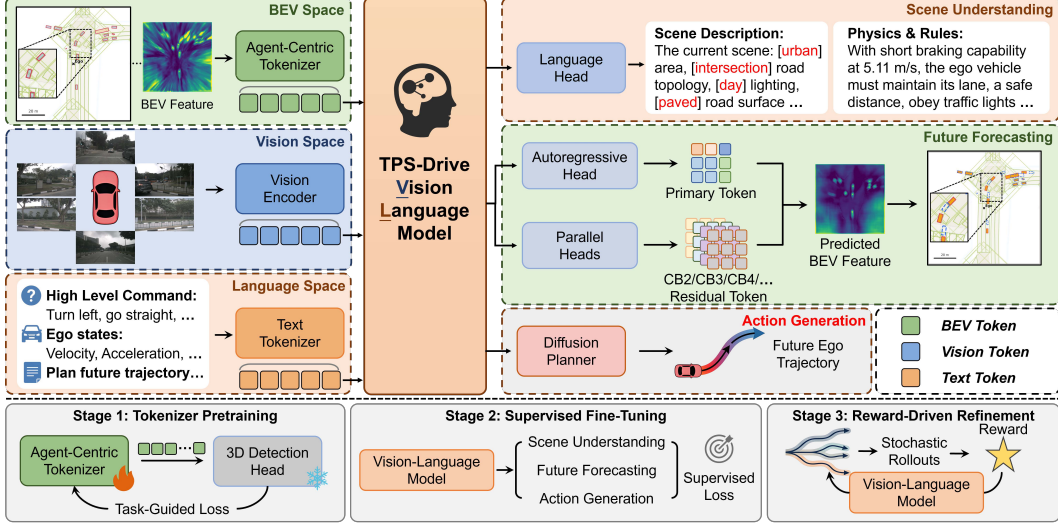


Figure 2: **Overview of TPS-Drive.** The decoupled VLM explicitly separates scene understanding, future forecasting, and action generation. The bottom panel illustrates the progressive three-stage training paradigm: tokenizer pretraining, supervised fine-tuning, and reward-driven refinement.

where D , H , and W denote the feature dimension and spatial resolutions. Alongside this visual context, the system receives a high-level navigation command c (e.g., *turn left*), a task prompt p , and current vehicle kinematics $\mathbf{k}_t = [\mathbf{v}_t, \mathbf{a}_t]$ comprising velocity and acceleration. The ultimate objective is to output a dynamically feasible future trajectory $\tau_{t+1:t+T_{\text{plan}}}$ over a planning horizon T_{plan} .

To effectively bridge these multimodal inputs and the continuous trajectory, we introduce an explicit intermediate representation. We construct a discrete spatial vocabulary \mathcal{V} via an agent-centric tokenizer (Sec. 3.2). Guided by a frozen 3D detection head, this vocabulary encodes the future BEV feature $\mathcal{B}_{t+\Delta t}$ into a distilled token sequence $\mathbf{z}_{t+\Delta t} \in \mathcal{V}^N$, where N denotes the sequence length. This tokenization explicitly isolates spatial redundancy while preserving the state of dynamic agents.

Grounded in this purified representation, the three-stage process operates sequentially: (1) **Scene Understanding:** A vision-language backbone first extracts \mathbf{s}_t , a unified structured representation encapsulating both the scene description and underlying physics rules from the current context. (2) **Future Forecasting:** Conditioned on \mathbf{s}_t and the current observations, the model predicts the future world tokens $\mathbf{z}_{t+\Delta t}$ to anticipate spatial evolution. (3) **Action Generation:** Finally, a conditional diffusion planner derives the continuous trajectory $\tau_{t+1:t+T_{\text{plan}}}$ based on these predicted states.

3.2 Agent-Centric Tokenization

Task-Guided Primary Codebook. The foundation of our spatial vocabulary is a primary codebook \mathcal{V}_1 , designed to extract the spatial states of dynamic agents from BEV features into discrete tokens. An encoder E_ϕ projects a BEV feature map \mathcal{B} into a lower-resolution latent grid $\mathbf{e} \in \mathbb{R}^{D' \times H' \times W'}$, where D' is the latent feature dimension and $H' \times W' = N$ defines the downsampled spatial resolution. Each spatial position $\mathbf{e}_{i,j} \in \mathbb{R}^{D'}$ is quantized to its nearest entry in \mathcal{V}_1 , producing a discrete token map $\mathbf{z} \in \mathcal{V}_1^N$:

$$z_{i,j} = \arg \min_m \|\mathbf{e}_{i,j} - \mathbf{v}_m\|_2, \quad \mathbf{q}_{i,j} = \mathbf{v}_{z_{i,j}}, \quad (1)$$

where $\mathbf{v}_m \in \mathbb{R}^{D'}$ is a codebook entry indexed by m , and $\mathbf{q} \in \mathbb{R}^{D' \times H' \times W'}$ is the quantized representation. A decoder D_ψ then reconstructs the purified feature map as $\hat{\mathcal{B}} = D_\psi(\mathbf{q})$.

To prevent this codebook from passively encoding task-irrelevant static background, we utilize a frozen, pretrained CenterPoint3D detection head[60, 61] for explicit supervision. The training objective balances reconstruction accuracy, task relevance, and codebook stability:

$$\mathcal{L}_{\text{primary}} = \underbrace{\lambda_r \mathcal{L}_{\text{rec}}(\hat{\mathcal{B}}, \mathcal{B})}_{\text{reconstruction}} + \underbrace{\lambda_h \mathcal{L}_{\text{hm}} + \lambda_b \mathcal{L}_{\text{box}}}_{\text{task guidance}} + \underbrace{\lambda_{\text{vq}} + \beta \mathcal{L}_{\text{commit}}}_{\text{codebook learning}}, \quad (2)$$

where \mathcal{L}_{hm} and \mathcal{L}_{box} denote the heatmap and 3D bounding box losses, respectively, and $\lambda_r, \lambda_h, \lambda_b, \beta$ are balancing weights. The terms \mathcal{L}_{vq} and $\mathcal{L}_{\text{commit}}$ represent standard VQ-VAE objectives [57]. While our primary objective is representation purification, the weighted reconstruction loss $\lambda_r \mathcal{L}_{\text{rec}}$ remains essential: although it may inadvertently preserve minor background details, it prevents the purified features from structurally deteriorating or deviating excessively from the original spatial distribution. This formulation compels \mathcal{V}_1 to learn a concise vocabulary of agent-centric patterns, enabling the vision-language backbone to effectively process spatial dynamics.

Residual Refinement Layers. Although the task-guided primary codebook captures core structural patterns, a single quantization level inherently loses precise positional nuances. To recover these details, we incorporate $L - 1$ supplementary codebooks, $\{\mathcal{V}_\ell\}_{\ell=2}^L$, arranged in a residual hierarchy. Each subsequent codebook quantizes the residual error from prior layers, producing L token maps $\{\mathbf{z}^{(\ell)}\}_{\ell=1}^L$ with corresponding quantized representations $\{\mathbf{q}^{(\ell)}\}_{\ell=1}^L$ that depict the purified BEV features at increasingly finer resolutions. The final high-fidelity reconstruction is obtained by decoding the cumulative quantized features: $\tilde{\mathbf{B}} = D_\psi(\sum_{\ell=1}^L \mathbf{q}^{(\ell)})$.

We refine this architecture through a two-phase optimization schedule. After training the primary codebook \mathcal{V}_1 , we freeze its weights and proceed to optimize the residual codebooks. Since \mathcal{V}_1 establishes a semantically comprehensive structural foundation, only the primary tokens $\mathbf{z}^{(1)}$ are input to the vision-language backbone as an autoregressive prediction target. The residual tokens are predicted in parallel using lightweight classification heads. This hierarchical structure keeps the autoregressive sequence compact for computational efficiency, while the residual layers retain high-fidelity spatial details.

3.3 Decoupled Reasoning Architecture

Scene Understanding. The first stage distills the driving environment into a unified structured representation \mathbf{s}_t , which encapsulates both a template-constrained scene description and underlying physics rules. Using a predefined vocabulary, this representation categorizes essential environmental attributes (e.g., *area type, road topology, lighting*) alongside explicit physical constraints (e.g., *short braking capability*). To obtain reliable supervision targets, we annotate the training data using the Qwen3.5-27B[62] model to generate the structured representations from raw sensor inputs and contextual metadata, followed by manual inspection to ensure correctness and consistency[63]. The resulting outputs are highly consistent, easily parsed, and supervised via a cross-entropy loss $\mathcal{L}_{\text{scene}}$ against these curated annotations. Crucially, because \mathbf{s}_t is generated prior to the future world tokens $\mathbf{z}_{t+\Delta t}$, it provides a comprehensive structured prior that conditions the subsequent spatial predictions.

Future Forecasting. The second stage forecasts the future spatial state within the discrete token space. Let $\mathbf{z}_{t+\Delta t}^{(1)}$ denote the primary tokens of the future purified BEV map at time $t + \Delta t$, and let $\{\mathbf{z}_{t+\Delta t}^{(\ell)}\}_{\ell=2}^L$ denote the corresponding residual tokens. The complete conditioning context is aggregated as $\mathbf{x}_t = \{\mathcal{I}_t, \mathcal{B}_t, \mathbf{c}, \mathbf{p}, \mathbf{k}_t, \mathbf{s}_t\}$. The vision-language backbone autoregressively predicts the primary token sequence in raster order[64] by modeling $p(z_{t+\Delta t, n}^{(1)} | \mathbf{x}_t, \mathbf{z}_{t+\Delta t, < n}^{(1)})$. Concurrently, $L - 1$ classification heads $\{g_\ell\}_{\ell=2}^L$ predict the residual tokens based on the hidden states $\mathbf{h}_{t+\Delta t}$ produced by the backbone during primary token generation. The overall objective combines autoregressive primary prediction with parallel residual classification:

$$\mathcal{L}_{\text{world}} = \underbrace{- \sum_{n=1}^N \log p(z_{t+\Delta t, n}^{(1)} | \mathbf{x}_t, \mathbf{z}_{t+\Delta t, < n}^{(1)})}_{\text{autoregressive primary}} + \underbrace{\lambda_{\text{res}} \sum_{\ell=2}^L \mathcal{L}_{\text{CE}}(g_\ell(\mathbf{h}_{t+\Delta t}), \mathbf{z}_{t+\Delta t}^{(\ell)})}_{\text{parallel residual}}, \quad (3)$$

where λ_{res} is a balancing weight and \mathcal{L}_{CE} denotes the standard cross-entropy loss.

Action Generation. The final stage translates the perceived environment and the anticipated agent positions into a continuous control trajectory. To effectively model the multi-modal distribution of human driving behaviors, we utilize a conditional diffusion model [65, 66]. The planner is conditioned on a unified feature vector \mathbf{f}_t , which concatenates the hidden states of the predicted future tokens $\mathbf{h}_{t+\Delta t}$, the structured representation \mathbf{s}_t , and an action start prompt $\mathbf{p}_{\text{start}}$. A denoising Transformer ϵ_θ is trained to estimate the noise injected during the forward diffusion process[67] by minimizing:

$$\mathcal{L}_{\text{plan}} = \mathbb{E}_{k, \tau^0, \epsilon} \left[\|\epsilon - \epsilon_\theta(\tau^k, k, \mathbf{f}_t)\|_2^2 \right], \quad (4)$$

Table 1: End-to-end trajectory planning experiments on nuScenes. * indicates that the ego status is additionally used. **Bold** and underline indicate the best and second-best VLM results. All average columns are highlighted in gray.

Method	ST-P3 metrics								UniAD metrics							
	L2 (m) ↓				CR (%) ↓				L2 (m) ↓				CR (%) ↓			
	1s	2s	3s	Avg.	1s	2s	3s	Avg.	1s	2s	3s	Avg.	1s	2s	3s	Avg.
<i>E2E-based Methods</i>																
ST-P3*[68] [ECCV'22]	1.33	2.11	2.90	2.11	0.23	0.62	1.27	0.71	-	-	-	-	-	-	-	-
UniAD*[69] [CVPR'23]	-	-	-	-	-	-	-	-	0.20	0.42	0.75	0.46	0.02	0.25	0.84	0.37
BEV-Planner[70] [CVPR'24]	0.30	0.52	0.83	0.55	0.10	0.37	1.30	0.59	-	-	-	-	-	-	-	-
BEV-Planner*[70] [CVPR'24]	0.16	0.32	0.57	0.35	0.00	0.29	0.73	0.34	-	-	-	-	-	-	-	-
MomAD[71] [CVPR'25]	0.31	0.57	0.91	0.60	0.01	0.05	0.22	0.09	0.43	0.88	1.62	0.98	0.06	0.16	0.68	0.30
HE-Drive[72] [ICLR'25]	0.31	0.58	0.93	0.61	0.01	0.05	0.16	0.07	-	-	-	-	-	-	-	-
DiffusionDrive[73] [CVPR'25]	0.31	0.62	1.03	0.65	0.03	0.06	0.19	0.09	0.43	1.01	1.83	1.09	0.05	0.14	0.55	0.25
PRIX[74] [RAL'26]	0.26	0.53	0.93	0.57	0.00	0.04	0.18	0.07	-	-	-	-	-	-	-	-
<i>VLM-based or World Model-based Methods</i>																
RDA-Driver*[75] [ECCV'24]	0.17	0.37	0.69	0.41	<u>0.01</u>	0.05	0.26	<u>0.11</u>	<u>0.23</u>	0.73	1.54	0.83	0.00	0.13	0.83	0.32
Doe-1[76] [arXiv'24]	0.37	0.67	1.07	0.70	0.02	0.14	0.47	0.21	0.50	1.18	2.11	1.26	0.04	0.37	1.19	0.53
OccWorld[12] [ECCV'24]	0.39	0.73	1.18	0.77	0.11	0.19	0.67	0.32	0.52	1.27	2.41	1.40	0.12	0.40	2.08	0.87
OmniDrive[27] [CVPR'25]	0.40	0.80	1.32	0.84	0.04	0.46	2.32	0.94	0.54	1.23	2.53	1.43	0.10	0.43	1.51	0.68
OmniDrive*[27] [CVPR'25]	0.14	<u>0.29</u>	0.55	0.33	0.00	0.13	0.78	0.30	0.25	0.49	1.11	0.62	<u>0.02</u>	0.13	0.65	0.27
EMMA*[77] [TMLR'25]	0.14	<u>0.29</u>	0.54	<u>0.32</u>	0.03	0.08	<u>0.25</u>	0.12	-	-	-	-	-	-	-	-
FSDrive[11] [NeurIPS'25]	0.28	0.52	0.80	0.53	0.06	0.13	0.32	0.17	0.40	0.89	1.60	0.96	0.07	0.12	1.02	0.40
FSDrive*[11] [NeurIPS'25]	0.14	0.25	0.46	0.28	0.03	<u>0.06</u>	0.21	0.10	0.18	<u>0.39</u>	0.77	0.45	0.00	<u>0.06</u>	<u>0.42</u>	<u>0.16</u>
TPS-Drive (Ours)	0.32	0.53	0.81	0.55	<u>0.01</u>	0.13	0.43	0.19	0.42	0.88	1.52	0.94	<u>0.02</u>	0.17	1.19	0.46
TPS-Drive* (Ours)	<u>0.15</u>	<u>0.29</u>	<u>0.53</u>	<u>0.32</u>	0.00	0.05	<u>0.25</u>	0.10	<u>0.23</u>	0.38	<u>0.85</u>	<u>0.49</u>	0.00	0.04	0.38	0.14

where $k \in \{1, \dots, K\}$ denotes the diffusion timestep, τ^0 is the ground-truth trajectory, $\epsilon \sim \mathcal{N}(\mathbf{0}, \mathbf{I})$ is the standard Gaussian noise sampled during the forward diffusion process, and τ^k represents the noised trajectory at step k . Optimizing the diffusion-based planner independently of the vision-language backbone significantly stabilizes training.

3.4 Training Strategy

We adopt a progressive three-stage training strategy that accommodates the distinct optimization dynamics of the tokenizer, vision-language backbone, and diffusion planner.

Stage 1: Tokenizer Pretraining. The spatial tokenizer is trained in two phases. First, the primary encoder E_ϕ , codebook \mathcal{V}_1 , and decoder D_ψ are optimized under the task-guided objective $\mathcal{L}_{\text{primary}}$. These components are then frozen while the residual codebooks $\{\mathcal{V}_\ell\}_{\ell=2}^L$ are trained under the reconstruction objective, yielding a universal and robust tokenizer.

Stage 2: Supervised Fine-Tuning. We adapt the pretrained vision-language backbone through supervised fine-tuning. The training objective jointly optimizes the three reasoning stages by combining $\mathcal{L}_{\text{scene}}$ for structured scene understanding, $\mathcal{L}_{\text{world}}$ (Eq. 3) for future world modeling, and $\mathcal{L}_{\text{plan}}$ (Eq. 4) for trajectory generation. The vision encoder and language model are fine-tuned efficiently, while the specialized projection, classification, and diffusion heads are fully updated.

Stage 3: Reward-Driven Refinement. To refine driving behavior beyond supervised imitation, we apply an end-to-end grouped relative optimization strategy[78]. For each sample, the policy generates multiple stochastic rollouts containing both predicted world tokens $\mathbf{z}_{t+\Delta t}$ and diffusion-generated trajectories τ , which are scored by an offline reward based on geometric errors and motion smoothness. Rewards are normalized within each group to form relative advantages, eliminating the need for a separate value network. The world-modeling branch is updated via an advantage-weighted policy objective, while the diffusion planner is refined through a reward-weighted denoising loss.

Table 2: Comparison on NAVSIMv1 with PDMS.

Method	Sensors	NC \uparrow	DAC \uparrow	TTC \uparrow	C \uparrow	EP \uparrow	PDMS \uparrow
Human	-	100.0	100.0	100.0	99.9	87.5	94.8
DiffusionDrive[73] [CVPR'25]	3 \times C + L	98.2	96.2	94.7	100.0	82.2	88.1
DrivingGPT[79] [ICCV'25]	1 \times C	98.9	90.7	94.9	95.6	79.7	82.4
WoTE[80] [ICCV'25]	3 \times C + L	98.5	96.8	94.4	99.9	81.9	88.3
AutoVLA[81] [NeurIPS'25]	3 \times C	98.4	95.6	98.0	99.9	81.9	89.1
Recogdrive[82] [ICLR'26]	3 \times C	98.2	97.8	95.2	99.8	83.5	89.6
TPS-Drive (Ours)	3 \times C	98.7	97.0	96.3	100.0	82.7	89.7

Table 3: Comparison on NAVSIMv2 with EPDMS.

Method	NC \uparrow	DAC \uparrow	DDC \uparrow	TLC \uparrow	EP \uparrow	TTC \uparrow	LK \uparrow	HC \uparrow	EC \uparrow	EPDMS \uparrow
TransFuser[83] [TPAMI'22]	96.9	89.9	97.8	99.7	87.1	95.4	92.7	98.3	87.2	76.7
Ego Status[70] [CVPR'24]	93.1	77.9	92.7	99.6	86.0	91.5	89.4	98.3	85.4	64.0
DiffusionDrive[73] [CVPR'25]	98.2	95.9	99.4	99.8	87.5	97.3	96.8	98.3	87.7	84.5
HydraMDP++[84] [CVPR'25]	98.5	98.5	99.5	99.7	87.4	97.9	95.8	98.2	75.7	85.6
DriveVLA-W0[85] [CVPR'25]	98.5	99.1	98.0	99.7	86.4	98.1	93.2	97.9	58.9	86.1
TPS-Drive (Ours)	98.5	98.6	99.7	99.8	87.6	98.0	97.1	98.3	82.5	86.7

4 Experiments

4.1 Experimental Setup

Datasets and Metrics. We evaluated TPS-Drive across three prominent autonomous driving benchmarks: nuScenes [88], NAVSIMv1 [89], and NAVSIMv2 [90]. For spatial forecasting and open-loop planning, we utilized the nuScenes dataset. Trajectory planning was assessed using L2 distance and Collision Rate (CR)[68, 69], while future world modeling was measured via the NuScenes Detection Score (NDS) and mean Average Precision (mAP) from agent-centric forecasts. To evaluate closed-loop interactive driving, we employed NAVSIMv1 and NAVSIMv2. NAVSIMv1 performance is captured by the Predictive Driver Model Score (PDMS), whereas NAVSIMv2 uses the Extended EPDMS to enforce stricter regulatory metrics, such as traffic light compliance.

Implementation Details. Our framework is built on the Qwen3.5-VL-2B[62] foundation model and trained using a progressive three-stage pipeline. The BEV encoder first compresses 200×200 spatial features to a 25×25 resolution. To discretize this space, we employ a primary codebook of 8,192 entries alongside $L = 4$ residual codebooks designed to capture fine-grained geometric details. Training begins with task-guided tokenizer pretraining, progresses to supervised fine-tuning of the decoupled architecture, and concludes with a stage of reward-driven refinement. This final stage optimizes the driving policy using simulated rewards to align the model with strict safety regulations.

4.2 Main Results

Open-Loop Planning (nuScenes). As summarized in Table 1, TPS-Drive establishes a new standard for collision avoidance among VLM-based autonomous driving models. The base model achieved a 0.19% CR under the ST-P3[68] protocol, substantially outperforming baselines such as OmniDrive[27] (0.94% CR) and OccWorld[12] (0.32% CR). When incorporating ego-status, TPS-Drive* achieved a record-low CR of 0.10% (ST-P3) and 0.14% (UniAD), effectively surpassing leading systems like FSDrive*[11]. These results validate that cleanly decoupling task-guided spatial understanding from continuous control effectively bridges the gap between high-level semantic reasoning and safe, precise maneuver generation.

Closed-Loop Planning (NAVSIM). The framework also demonstrated exceptional robustness in interactive, closed-loop environments. On NAVSIMv1 (Table 2), TPS-Drive achieved a PDMS of 89.7, surpassing recent top-performing models such as Recogdrive[82] (89.6) and AutoVLA[81] (89.1).

Table 4: Evaluation of agent spatial forecasting on nuScenes.

Method	NDS (%) \uparrow	mAP (%) \uparrow	mATE \downarrow	mASE \downarrow	mAOE \downarrow	mAVE \downarrow	mAAE \downarrow
BEVWorld[86] [arXiv'24]	25.72	21.03	0.647	0.526	0.848	1.179	0.461
Drive-OccWorld[87] [AAAI'25]	20.80	20.20	0.739	0.761	0.865	1.069	0.565
WoTE[80] [ICCV'25]	30.01	22.77	0.653	0.534	0.757	0.839	0.388
TPS-Drive (Ours)	34.60	24.03	0.610	0.421	0.704	0.725	0.300

Table 5: Ablation studies on the core components of TPS-Drive.

TPS-Drive Components			World Model	Planning Metrics		
Task-Guided Tokenizer	Residual Layers ($L = 4$)	Reward-Driven Refinement	NDS (%) \uparrow	L2 (m) \downarrow	CR (%) \downarrow	EPDMS \uparrow
			17.31	0.64	0.33	81.1
\checkmark			30.03	0.63	0.28	83.7
\checkmark	\checkmark		33.78	0.61	0.26	84.1
\checkmark	\checkmark	\checkmark	34.60	0.55	0.19	86.7

On the more rigorous NAVSIMv2 platform (Table 3), it attained an EPDMS of 86.7, outperforming both concurrent VLA methods like DriveVLA-W0[85] (86.1) and expert-level planners such as HydraMDP++[84] (85.6). Notably, the model maintained high scores across granular regulatory metrics, including 99.8% for traffic light compliance and 97.1% for lane keeping.

Agent-Centric Spatial Reasoning. To verify the depth of our model’s spatial reasoning, we evaluated its agent-centric forecasting accuracy on nuScenes (Table 4). By feeding predicted BEV features into a fine-tuned detection head, TPS-Drive achieved 34.60% NDS and 24.03% mAP. This performance significantly improves upon established world models such as WoTE[80] (30.01% NDS) and BEVWorld[86] (25.72% NDS). These accuracy gains confirm the model reliably predicts future states, ensuring a stable foundation for downstream planning.

4.3 Ablation Studies

We systematically validate the architectural design of TPS-Drive by progressively introducing its core components, as detailed in Table 5.

Effect of Task-Guided Tokenization. Our baseline utilizes a standard reconstruction-guided VQ-VAE[57] without task-specific supervision. This approach forces the model to encode massive amounts of task-irrelevant background, leading to representation interference, poor spatial reasoning (17.31% NDS), and suboptimal closed-loop planning (81.1 EPDMS). By introducing the Task-Guided Primary Tokenizer, we explicitly filter out static backgrounds to focus purely on critical dynamic agents. This "representation purification" yields a +12.72% absolute increase in forecasting accuracy (reaching 30.03% NDS) and improves the EPDMS to 83.7. This confirms that isolating safety-critical semantics from raw visual data is foundational for effective reasoning in VLA models.

Effect of Residual Refinement Layers. While the purified primary tokenizer establishes a robust semantic foundation, incorporating $L = 4$ residual codebooks substantially enhances the model’s ability to capture fine-grained geometric and kinematic details. This hierarchical quantization yields an additional +3.75% absolute boost in spatial forecasting accuracy (reaching 33.78% NDS). Because the downstream diffusion planner relies on this enriched spatial vocabulary[91, 92], open-loop planning safety naturally improves, with the ST-P3 Collision Rate (CR) dropping from 0.28% to 0.26% and the L2 error decreasing to 0.61m.

Effect of Reward-Driven Refinement. The final training stage is essential for aligning the generalized spatial representation with strict, real-world driving regulations[93, 94]. Applying policy optimization driven by simulated rewards boosts the NAVSIMv2 EPDMS from 84.1 to 86.7. Furthermore, the open-loop collision rate undergoes a drastic reduction to 0.19%. Interestingly, this

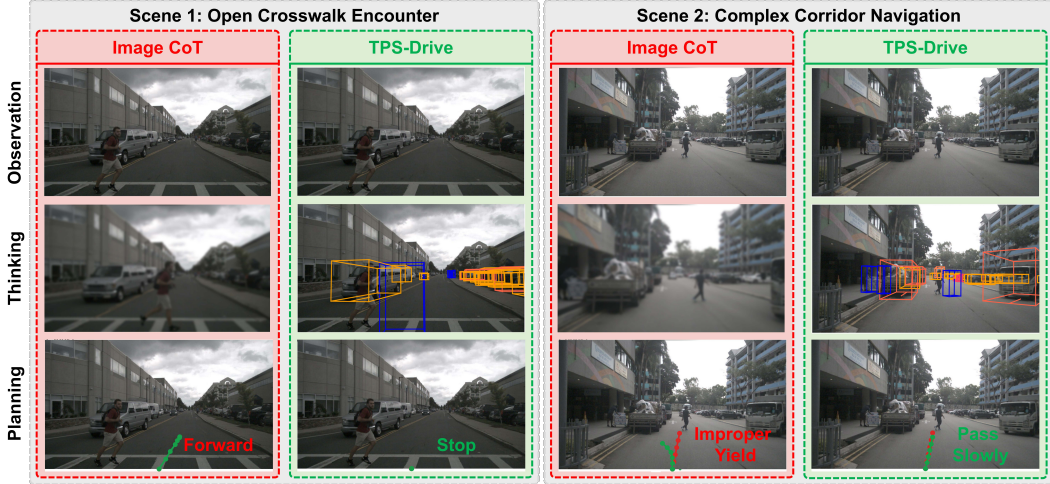


Figure 3: **Qualitative comparison in safety-critical scenarios.** Rows denote visual **Observation**, internal **Thinking**, and trajectory **Planning**. In Planning, **green** and **red** indicate predicted and ground-truth trajectories, respectively. **Left:** Facing a pedestrian, the baseline wrongly plans "Forward", while TPS-Drive explicitly predicts 3D bounding boxes to safely "Stop". **Right:** In a cluttered corridor, the baseline makes an "Improper Yield", whereas TPS-Drive accurately aligns with the ground truth to "Pass Slowly".

policy-level alignment synergistically improves the upstream world modeling quality (NDS increases to 34.60%), proving that continuous planning rewards effectively encourage the discrete representations to prioritize safety-critical spatial features.

4.4 Qualitative Analysis

Figure 3 contrasts TPS-Drive with an implicit Image Chain-of-Thought (CoT) baseline [11] in safety-critical driving scenarios. Relying on dense image representations, the baseline model suffers from severe representation interference. Overwhelmed by redundant background noise, its semantic reasoning fails to accurately identify task-critical dynamic hazards, leading to dangerous maneuvers. Specifically, the baseline dangerously plans to drive "Forward" into a crossing pedestrian (Scene 1) and executes an "Improper Yield" in a cluttered corridor (Scene 2).

Conversely, TPS-Drive overcomes these limitations by explicitly forecasting the 3D bounding boxes of surrounding agents. By reasoning within this task-guided, purified spatial vocabulary, our planner accurately interprets complex geometric constraints. It successfully isolates critical dynamic agents from background redundancy to synthesize safe and compliant trajectories, such as executing a timely "Stop" (Scene 1) and deciding to "Pass Slowly" (Scene 2). This confirms that explicit tokenization significantly enhances both interpretability and driving safety.

5 Conclusion

We propose TPS-Drive, a decoupled framework designed to overcome spatial hallucinations and representation interference in VLM-based autonomous driving. By employing a frozen 3D detection head to supervise the task-guided vector quantization process, our Agent-Centric Tokenizer distills critical dynamic agents from redundant backgrounds into a purified spatial vocabulary. Consequently, TPS-Drive delivers exceptional open-loop spatial forecasting accuracy and establishes new safety records on closed-loop interactive benchmarks, validating that purified geometric representations effectively bridge the gap between high-level semantic reasoning and safe trajectory generation.

Limitations and Future Work. Relying on a frozen detection head bounds representation potential, and the decoupled multi-stage architecture currently restricts real-time inference speed. Future work will explore end-to-end differentiable spatial purification and optimize deployment on dedicated hardware accelerators for low-latency autonomous control.

References

- [1] Sicong Jiang, Zilin Huang, Kangan Qian, Ziang Luo, Tianze Zhu, Yang Zhong, Yihong Tang, Menglin Kong, Yunlong Wang, Siwen Jiao, et al. A survey on vision-language-action models for autonomous driving. In *Proceedings of the IEEE/CVF International Conference on Computer Vision*, pages 4524–4536, 2025.
- [2] Xingcheng Zhou, Mingyu Liu, Ekim Yurtsever, Bare Luka Zagar, Walter Zimmer, Hu Cao, and Alois C Knoll. Vision language models in autonomous driving: A survey and outlook. *IEEE Transactions on Intelligent Vehicles*, 2024.
- [3] Hanlin Tian, Kethan Reddy, Yuxiang Feng, Mohammed Quddus, Yiannis Demiris, and Panagiotis Angeloudis. Large (vision) language models for autonomous vehicles: Current trends and future directions. *IEEE Transactions on Intelligent Transportation Systems*, 27(1):187–210, 2025.
- [4] Jie Wang, Guang Li, Zhijian Huang, Chenxu Dang, Hangjun Ye, Yahong Han, and Long Chen. Vggdrive: Empowering vision-language models with cross-view geometric grounding for autonomous driving. *arXiv preprint arXiv:2602.20794*, 2026.
- [5] Shijie Zhou, Alexander Vilesov, Xuehai He, Ziyu Wan, Shuwang Zhang, Aditya Nagachandra, Di Chang, Dongdong Chen, Xin Eric Wang, and Achuta Kadambi. Vlm4d: Towards spatiotemporal awareness in vision language models. In *Proceedings of the IEEE/CVF international conference on computer vision*, pages 8600–8612, 2025.
- [6] Xianda Guo, Ruijun Zhang, Yiqun Duan, Yuhang He, Dujun Nie, Wenke Huang, Chenming Zhang, Shuai Liu, Hao Zhao, and Long Chen. Surds: Benchmarking spatial understanding and reasoning in driving scenarios with vision language models. *arXiv preprint arXiv:2411.13112*, 2024.
- [7] Dongming Wu, Wencheng Han, Yingfei Liu, Tiancai Wang, Cheng-zhong Xu, Xiangyu Zhang, and Jianbing Shen. Language prompt for autonomous driving. In *Proceedings of the AAAI conference on artificial intelligence*, volume 39, pages 8359–8367, 2025.
- [8] Linfeng He, Yiming Sun, Sihao Wu, Jiayu Liu, and Xiaowei Huang. Integrating object detection modality into visual language model for enhanced autonomous driving agent. *arXiv preprint arXiv:2411.05898*, 2024.
- [9] Peizheng Li, Zhenghao Zhang, David Holtz, Hang Yu, Yutong Yang, Yuzhi Lai, Rui Song, Andreas Geiger, and Andreas Zell. Spacedrive: Infusing spatial awareness into vlm-based autonomous driving. *arXiv preprint arXiv:2512.10719*, 2, 2025.
- [10] Yuechen Luo, Fang Li, Shaoqing Xu, Yang Ji, Zehan Zhang, Bing Wang, Yuannan Shen, Jianwei Cui, Long Chen, Guang Chen, et al. Last-vla: Thinking in latent spatio-temporal space for vision-language-action in autonomous driving. *arXiv preprint arXiv:2603.01928*, 2026.
- [11] Shuang Zeng, Xinyuan Chang, Mengwei Xie, Xinran Liu, Yifan Bai, Zheng Pan, Mu Xu, Xing Wei, and Ning Guo. Futuresightdrive: Thinking visually with spatio-temporal cot for autonomous driving. *arXiv preprint arXiv:2505.17685*, 2025.
- [12] Wenzhao Zheng, Weiliang Chen, Yuanhui Huang, Borui Zhang, Yueqi Duan, and Jiwen Lu. Occworld: Learning a 3d occupancy world model for autonomous driving. In *European conference on computer vision*, pages 55–72. Springer, 2024.
- [13] Jiajun Cao, Qizhe Zhang, Peidong Jia, Xuhui Zhao, Bo Lan, Xiaohan Zhang, Xiaobao Wei, Sixiang Chen, Liyun Li, Xianming Liu, et al. Fastdrivevla: Efficient end-to-end driving via plug-and-play reconstruction-based token pruning. In *Proceedings of the AAAI Conference on Artificial Intelligence*, volume 40, pages 2571–2579, 2026.
- [14] Yongshuo Zong, Oisin Mac Aodha, and Timothy M Hospedales. Self-supervised multi-modal learning: A survey. *IEEE Transactions on Pattern Analysis and Machine Intelligence*, 47(7):5299–5318, 2024.

- [15] Mustafa Shukor, Enrico Fini, Victor Guilherme Turrisi da Costa, Matthieu Cord, Joshua Susskind, and Alaaeldin El-Nouby. Scaling laws for native multimodal models. In *Proceedings of the IEEE/CVF International Conference on Computer Vision*, pages 12–23, 2025.
- [16] Zhenjie Yang, Xiaosong Jia, Hongyang Li, and Junchi Yan. Llm4drive: A survey of large language models for autonomous driving. *arXiv preprint arXiv:2311.01043*, 2023.
- [17] Chonghao Sima, Katrin Renz, Kashyap Chitta, Li Chen, Hanxue Zhang, Chengen Xie, Jens Beißwenger, Ping Luo, Andreas Geiger, and Hongyang Li. Drivelm: Driving with graph visual question answering. In *European conference on computer vision*, pages 256–274. Springer, 2024.
- [18] Christian Fruhwirth-Reisinger, Dušan Malić, Wei Lin, David Schinagl, Samuel Schuller, and Horst Possegger. Stsbench: A spatio-temporal scenario benchmark for multi-modal large language models in autonomous driving. *arXiv preprint arXiv:2506.06218*, 2025.
- [19] Roberto Brusnicki, Mattia Piccinini, and Johannes Betz. How well do vision-language models understand sequential driving scenes? a sensitivity study. *arXiv preprint arXiv:2604.06750*, 2026.
- [20] Tong Zeng, Longfeng Wu, Liang Shi, Dawei Zhou, and Feng Guo. Are vision llms road-ready? a comprehensive benchmark for safety-critical driving video understanding. In *Proceedings of the 31st ACM SIGKDD Conference on Knowledge Discovery and Data Mining V. 2*, pages 5972–5983, 2025.
- [21] Zhenhua Xu, Yujia Zhang, Enze Xie, Zhen Zhao, Yong Guo, Kwan-Yee K Wong, Zhenguo Li, and Hengshuang Zhao. Drivegpt4: Interpretable end-to-end autonomous driving via large language model. *IEEE Robotics and Automation Letters*, 9(10):8186–8193, 2024.
- [22] Hao Shao, Yuxuan Hu, Letian Wang, Guanglu Song, Steven L Waslander, Yu Liu, and Hongsheng Li. Lmdrive: Closed-loop end-to-end driving with large language models. In *Proceedings of the IEEE/CVF conference on computer vision and pattern recognition*, pages 15120–15130, 2024.
- [23] Xiaosong Jia, Zhenjie Yang, Qifeng Li, Zhiyuan Zhang, and Junchi Yan. Bench2drive: Towards multi-ability benchmarking of closed-loop end-to-end autonomous driving. *Advances in Neural Information Processing Systems*, 37:819–844, 2024.
- [24] Xiaosong Jia, Yuqian Shao, Zhenjie Yang, Qifeng Li, Zhiyuan Zhang, and Junchi Yan. Bench2drive-vl: Benchmarks for closed-loop autonomous driving with vision-language models. *arXiv preprint arXiv:2604.01259*, 2026.
- [25] Alexey Dosovitskiy, German Ros, Felipe Codevilla, Antonio Lopez, and Vladlen Koltun. Carla: An open urban driving simulator. In *Conference on robot learning*, pages 1–16. PMLR, 2017.
- [26] Erfei Cui, Wenhai Wang, Zhiqi Li, Jiangwei Xie, Haoming Zou, Hanming Deng, Gen Luo, Lewei Lu, Xizhou Zhu, and Jifeng Dai. Drivemlm: aligning multi-modal large language models with behavioral planning states for autonomous driving. *Visual Intelligence*, 3(1):22, 2025.
- [27] Shihao Wang, Zhiding Yu, Xiaohui Jiang, Shiyi Lan, Min Shi, Nadine Chang, Jan Kautz, Ying Li, and Jose M Alvarez. Omnidrive: A holistic vision-language dataset for autonomous driving with counterfactual reasoning. In *Proceedings of the computer vision and pattern recognition conference*, pages 22442–22452, 2025.
- [28] Katharina Winter, Mark Azer, and Fabian B Flohr. Bevdriver: Leveraging bev maps in llms for robust closed-loop driving. In *2025 IEEE/RSJ International Conference on Intelligent Robots and Systems (IROS)*, pages 20379–20385. IEEE, 2025.
- [29] Ruixun Liu, Lingyu Kong, Derun Li, and Hang Zhao. Occvla: Vision-language-action model with implicit 3d occupancy supervision. *arXiv preprint arXiv:2509.05578*, 2025.
- [30] Yuchen Li, Amanmeet Garg, Shalini Chaudhuri, Rui Zhao, and Garin Kessler. Perceptio: Perception enhanced vision language models via spatial token generation. *arXiv preprint arXiv:2603.18795*, 2026.

- [31] Makanjuola Ogunleye, Eman Abdelrahman, and Ismini Lourentzou. 3d-vcd: Hallucination mitigation in 3d-llm embodied agents through visual contrastive decoding. *arXiv preprint arXiv:2604.08645*, 2026.
- [32] Jiaqi Fan, Jianhua Wu, Hongqing Chu, Quanbo Ge, and Bingzhao Gao. Hallucination elimination and semantic enhancement framework for vision-language models in traffic scenarios. *arXiv preprint arXiv:2412.07518*, 2024.
- [33] Sai Bhargav Rongali, Aadya Pipersenia, and Kenji Okuma. Task interference in vlms for autonomous driving: When better perception hurts planning. In *AAAI 2026 Workshop on Assessing and Improving Reliability of Foundation Models in the Real World*.
- [34] Xiaolu Liu, Yicong Li, Song Wang, Junbo Chen, Angela Yao, and Jianke Zhu. Dynflowdrive: Flow-based dynamic world modeling for autonomous driving. *arXiv preprint arXiv:2603.19675*, 2026.
- [35] Sifan Tu, Xin Zhou, Dingkang Liang, Xingyu Jiang, Yumeng Zhang, Xiaofan Li, and Xiang Bai. The role of world models in shaping autonomous driving: A comprehensive survey. *arXiv preprint arXiv:2502.10498*, 2025.
- [36] Yupeng Zheng, Pengxuan Yang, Zebin Xing, Qichao Zhang, Yuhang Zheng, Yinfeng Gao, Pengfei Li, Teng Zhang, Zhongpu Xia, Peng Jia, et al. World4drive: End-to-end autonomous driving via intention-aware physical latent world model. In *Proceedings of the IEEE/CVF International Conference on Computer Vision*, pages 28632–28642, 2025.
- [37] Tuo Feng, Wenguan Wang, and Yi Yang. A survey of world models for autonomous driving. *arXiv preprint arXiv:2501.11260*, 2025.
- [38] Christopher Diehl, Quinlan Sykora, Ben Agro, Thomas Gilles, Sergio Casas, and Raquel Urtasun. Dio: Decomposable implicit 4d occupancy-flow world model. In *Proceedings of the Computer Vision and Pattern Recognition Conference*, pages 27456–27466, 2025.
- [39] Chuyao Fu, Shengzhe Gan, Zhuoli Ouyang, Yuhan Rui, Xiaowei Chi, Sirui Han, Jiankun Wang, and Hong Zhang. Prodrive: Proactive planning for autonomous driving via ego-environment co-evolution. *arXiv preprint arXiv:2604.25329*, 2026.
- [40] Zetong Yang, Li Chen, Yanan Sun, and Hongyang Li. Visual point cloud forecasting enables scalable autonomous driving. In *Proceedings of the IEEE/CVF Conference on Computer Vision and Pattern Recognition*, pages 14673–14684, 2024.
- [41] Ben Agro, Quinlan Sykora, Sergio Casas, Thomas Gilles, and Raquel Urtasun. Uno: Unsupervised occupancy fields for perception and forecasting. In *Proceedings of the IEEE/CVF Conference on Computer Vision and Pattern Recognition*, pages 14487–14496, 2024.
- [42] Songen Gu, Wei Yin, Bu Jin, Xiaoyang Guo, Junming Wang, Haodong Li, Qian Zhang, and Xiaoxiao Long. Dome: Taming diffusion model into high-fidelity controllable occupancy world model. *arXiv preprint arXiv:2410.10429*, 2024.
- [43] Chen Min, Dawei Zhao, Liang Xiao, Jian Zhao, Xinli Xu, Zheng Zhu, Lei Jin, Jianshu Li, Yulan Guo, Junliang Xing, et al. Driveworld: 4d pre-trained scene understanding via world models for autonomous driving. In *Proceedings of the IEEE/CVF conference on computer vision and pattern recognition*, pages 15522–15533, 2024.
- [44] Wei Wu, Xiaoxin Feng, Ziyang Gao, and Yuheng Kan. Smart: Scalable multi-agent real-time motion generation via next-token prediction. *Advances in Neural Information Processing Systems*, 37:114048–114071, 2024.
- [45] Tom Brown, Benjamin Mann, Nick Ryder, Melanie Subbiah, Jared D Kaplan, Prafulla Dhariwal, Arvind Neelakantan, Pranav Shyam, Girish Sastry, Amanda Askell, et al. Language models are few-shot learners. *Advances in neural information processing systems*, 33:1877–1901, 2020.
- [46] Anthony Hu, Lloyd Russell, Hudson Yeo, Zak Murez, George Fedoseev, Alex Kendall, Jamie Shotton, and Gianluca Corrado. Gaia-1: A generative world model for autonomous driving. *arXiv preprint arXiv:2309.17080*, 2023.

- [47] Anthony Hu, Gianluca Corrado, Nicolas Griffiths, Zachary Murez, Corina Gurau, Hudson Yeo, Alex Kendall, Roberto Cipolla, and Jamie Shotton. Model-based imitation learning for urban driving. *Advances in Neural Information Processing Systems*, 35:20703–20716, 2022.
- [48] Jake Bruce, Michael D Dennis, Ashley Edwards, Jack Parker-Holder, Yuge Shi, Edward Hughes, Matthew Lai, Aditi Mavalankar, Richie Steigerwald, Chris Apps, et al. Genie: Generative interactive environments. In *Forty-first International Conference on Machine Learning*, 2024.
- [49] Danijar Hafner, Jurgis Pasukonis, Jimmy Ba, and Timothy Lillicrap. Mastering diverse domains through world models. *arXiv preprint arXiv:2301.04104*, 2023.
- [50] Patrick Esser, Robin Rombach, and Bjorn Ommer. Taming transformers for high-resolution image synthesis. In *Proceedings of the IEEE/CVF conference on computer vision and pattern recognition*, pages 12873–12883, 2021.
- [51] Chuofan Ma, Yi Jiang, Junfeng Wu, Jihan Yang, Xin Yu, Zehuan Yuan, Bingyue Peng, and Xiaojuan Qi. Unitok: A unified tokenizer for visual generation and understanding. *arXiv preprint arXiv:2502.20321*, 2025.
- [52] Boyuan Chen, Zhuo Xu, Sean Kirmani, Brain Ichter, Dorsa Sadigh, Leonidas Guibas, and Fei Xia. Spatialvlm: Endowing vision-language models with spatial reasoning capabilities. In *Proceedings of the IEEE/CVF Conference on Computer Vision and Pattern Recognition*, pages 14455–14465, 2024.
- [53] Jiacheng Hua, Yishu Yin, Yuhang Wu, Tai Wang, Yifei Huang, and Miao Liu. Unleashing spatial reasoning in multimodal large language models via textual representation guided reasoning. *arXiv preprint arXiv:2603.23404*, 2026.
- [54] Jiangye Yuan, Gowri Kumar, and Baoyuan Wang. Boosting mllm spatial reasoning with geometrically referenced 3d scene representations. *arXiv preprint arXiv:2603.08592*, 2026.
- [55] Anna-Maria Halacheva, Jan-Nico Zaech, Xi Wang, Danda Pani Paudel, and Luc Van Gool. Gaussianvlm: Scene-centric 3d vision-language models using language-aligned gaussian splats for embodied reasoning and beyond. *IEEE Robotics and Automation Letters*, 2025.
- [56] An-Chieh Cheng, Hongxu Yin, Yang Fu, Qiushan Guo, Ruihan Yang, Jan Kautz, Xiaolong Wang, and Sifei Liu. Spatialrgpt: Grounded spatial reasoning in vision-language models. *Advances in Neural Information Processing Systems*, 37:135062–135093, 2024.
- [57] Aaron Van Den Oord, Oriol Vinyals, et al. Neural discrete representation learning. *Advances in neural information processing systems*, 30, 2017.
- [58] Julong Wei, Shanshuai Yuan, Pengfei Li, Qingda Hu, Zhongxue Gan, and Wenchao Ding. Occllama: An occupancy-language-action generative world model for autonomous driving. *arXiv preprint arXiv:2409.03272*, 2024.
- [59] Zhiqi Li, Wenhai Wang, Hongyang Li, Enze Xie, Chonghao Sima, Tong Lu, Qiao Yu, and Jifeng Dai. Bevformer: learning bird’s-eye-view representation from lidar-camera via spatiotemporal transformers. *IEEE Transactions on Pattern Analysis and Machine Intelligence*, 47(3):2020–2036, 2024.
- [60] Tianwei Yin, Xingyi Zhou, and Philipp Krahenbuhl. Center-based 3d object detection and tracking. In *Proceedings of the IEEE/CVF conference on computer vision and pattern recognition*, pages 11784–11793, 2021.
- [61] Yin Zhou and Oncel Tuzel. Voxelnet: End-to-end learning for point cloud based 3d object detection. In *Proceedings of the IEEE conference on computer vision and pattern recognition*, pages 4490–4499, 2018.
- [62] Qwen Team. Qwen3. 5-omni technical report. *arXiv preprint arXiv:2604.15804*, 2026.
- [63] Shuo Liu, Lei Shi, Yucheng Shi, Yufei Gao, and Xiaole Sun. Traffic scene perception via multimodal large language model with data augmentation and efficient training strategy. *Applied Soft Computing*, 177:113210, 2025.

- [64] Payel Dutta and Kaustuv Kunal. Implementation of image generative models using imagegpt. In *2023 International Conference on New Frontiers in Communication, Automation, Management and Security (ICCAMS)*, volume 1, pages 1–6. IEEE, 2023.
- [65] Lvmin Zhang, Anyi Rao, and Maneesh Agrawala. Adding conditional control to text-to-image diffusion models. In *Proceedings of the IEEE/CVF international conference on computer vision*, pages 3836–3847, 2023.
- [66] Bingyi Kang, Xiao Ma, Chao Du, Tianyu Pang, and Shuicheng Yan. Efficient diffusion policies for offline reinforcement learning. *Advances in Neural Information Processing Systems*, 36:67195–67212, 2023.
- [67] Jonathan Ho, Ajay Jain, and Pieter Abbeel. Denoising diffusion probabilistic models. *Advances in neural information processing systems*, 33:6840–6851, 2020.
- [68] Shengchao Hu, Li Chen, Penghao Wu, Hongyang Li, Junchi Yan, and Dacheng Tao. St-p3: End-to-end vision-based autonomous driving via spatial-temporal feature learning. In *European Conference on Computer Vision*, pages 533–549. Springer, 2022.
- [69] Yihan Hu, Jiazhi Yang, Li Chen, Keyu Li, Chonghao Sima, Xizhou Zhu, Siqi Chai, Senyao Du, Tianwei Lin, Wenhai Wang, et al. Planning-oriented autonomous driving. In *Proceedings of the IEEE/CVF conference on computer vision and pattern recognition*, pages 17853–17862, 2023.
- [70] Zhiqi Li, Zhiding Yu, Shiyi Lan, Jiahao Li, Jan Kautz, Tong Lu, and Jose M Alvarez. Is ego status all you need for open-loop end-to-end autonomous driving? In *Proceedings of the IEEE/CVF Conference on Computer Vision and Pattern Recognition*, pages 14864–14873, 2024.
- [71] Ziyang Song, Caiyan Jia, Lin Liu, Hongyu Pan, Yongchang Zhang, Junming Wang, Xingyu Zhang, Shaoqing Xu, Lei Yang, and Yadan Luo. Don’t shake the wheel: Momentum-aware planning in end-to-end autonomous driving. In *Proceedings of the IEEE/CVF Conference on Computer Vision and Pattern Recognition*, pages 22432–22441, 2025.
- [72] Junming Wang, Xingyu Zhang, Zebin Xing, Xiaoyang Guo, Yang Hu, Ziyang Song, Qian Zhang, Xiaoxiao Long, Wei Yin, et al. He-drive: Human-like end-to-end driving with vision language models. 2024.
- [73] Bencheng Liao, Shaoyu Chen, Haoran Yin, Bo Jiang, Cheng Wang, Sixu Yan, Xinbang Zhang, Xiangyu Li, Ying Zhang, Qian Zhang, et al. Diffusiondrive: Truncated diffusion model for end-to-end autonomous driving. In *Proceedings of the Computer Vision and Pattern Recognition Conference*, pages 12037–12047, 2025.
- [74] Maciej Wozniak, Lianhang Liu, Yixi Cai, and Patric Jensfelt. Prix: learning to plan from raw pixels for end-to-end autonomous driving. *IEEE Robotics and Automation Letters*, 11(5):6400–6407, 2026.
- [75] Zhijian Huang, Tao Tang, Shaoxiang Chen, Sihao Lin, Zequn Jie, Lin Ma, Guangrun Wang, and Xiaodan Liang. Making large language models better planners with reasoning-decision alignment. In *European Conference on Computer Vision*, pages 73–90. Springer, 2024.
- [76] Wenzhao Zheng, Zetian Xia, Yuanhui Huang, Sicheng Zuo, Jie Zhou, and Jiwen Lu. Doe-1: Closed-loop autonomous driving with large world model. *arXiv preprint arXiv:2412.09627*, 2024.
- [77] Jyh-Jing Hwang, Runsheng Xu, Hubert Lin, Wei-Chih Hung, Jingwei Ji, Kristy Choi, Di Huang, Tong He, Paul Covington, Benjamin Sapp, et al. Emma: End-to-end multimodal model for autonomous driving. *arXiv preprint arXiv:2410.23262*, 2024.
- [78] Zhihong Shao, Peiyi Wang, Qihao Zhu, Runxin Xu, Junxiao Song, Xiao Bi, Haowei Zhang, Mingchuan Zhang, YK Li, Yang Wu, et al. Deepseekmath: Pushing the limits of mathematical reasoning in open language models. *arXiv preprint arXiv:2402.03300*, 2024.

- [79] Yuntao Chen, Yuqi Wang, and Zhaoxiang Zhang. Drivingsgpt: Unifying driving world modeling and planning with multi-modal autoregressive transformers. In *Proceedings of the IEEE/CVF International Conference on Computer Vision*, pages 26890–26900, 2025.
- [80] Yingyan Li, Yuqi Wang, Yang Liu, Jiawei He, Lue Fan, and Zhaoxiang Zhang. End-to-end driving with online trajectory evaluation via bev world model. In *Proceedings of the IEEE/CVF International Conference on Computer Vision*, pages 27137–27146, 2025.
- [81] Zewei Zhou, Tianhui Cai, Seth Z Zhao, Yun Zhang, Zhiyu Huang, Bolei Zhou, and Jiaqi Ma. Autovla: A vision-language-action model for end-to-end autonomous driving with adaptive reasoning and reinforcement fine-tuning. *arXiv preprint arXiv:2506.13757*, 2025.
- [82] Yongkang Li, Kaixin Xiong, Xiangyu Guo, Fang Li, Sixu Yan, Gangwei Xu, Lijun Zhou, Long Chen, Haiyang Sun, Bing Wang, et al. Recogdrive: A reinforced cognitive framework for end-to-end autonomous driving. *arXiv preprint arXiv:2506.08052*, 2025.
- [83] Kashyap Chitta, Aditya Prakash, Bernhard Jaeger, Zehao Yu, Katrin Renz, and Andreas Geiger. Transfuser: Imitation with transformer-based sensor fusion for autonomous driving. *IEEE transactions on pattern analysis and machine intelligence*, 45(11):12878–12895, 2022.
- [84] Kailin Li, Zhenxin Li, Shiyi Lan, Jiayi Liu, Yuan Xie, Zuxuan Wu, Zhiding Yu, Jose M Alvarez, et al. Hydra-mdp++: Advancing end-to-end driving via hydra-distillation with expert-guided decision analysis. 2025.
- [85] Yingyan Li, Shuyao Shang, Weisong Liu, Bing Zhan, Haochen Wang, Yuqi Wang, Yuntao Chen, Xiaoman Wang, Yasong An, Chufeng Tang, et al. Drivevla-w0: World models amplify data scaling law in autonomous driving. *arXiv preprint arXiv:2510.12796*, 2025.
- [86] Yumeng Zhang, Shi Gong, Kaixin Xiong, Xiaoqing Ye, Xiao Tan, Fan Wang, Jizhou Huang, Hua Wu, and Haifeng Wang. Bevworld: A multimodal world model for autonomous driving via unified bev latent space. 2024.
- [87] Yu Yang, Jianbiao Mei, Yukai Ma, Siliang Du, Wenqing Chen, Yijie Qian, Yuxiang Feng, and Yong Liu. Driving in the occupancy world: Vision-centric 4d occupancy forecasting and planning via world models for autonomous driving. In *Proceedings of the AAAI Conference on Artificial Intelligence*, volume 39, pages 9327–9335, 2025.
- [88] Holger Caesar, Varun Bankiti, Alex H Lang, Sourabh Vora, Venice Erin Liong, Qiang Xu, Anush Krishnan, Yu Pan, Giancarlo Baldan, and Oscar Beijbom. nuscenes: A multimodal dataset for autonomous driving. In *Proceedings of the IEEE/CVF conference on computer vision and pattern recognition*, pages 11621–11631, 2020.
- [89] Daniel Dauner, Marcel Hallgarten, Tianyu Li, Xinshuo Weng, Zhiyu Huang, Zetong Yang, Hongyang Li, Igor Gilitschenski, Boris Ivanovic, Marco Pavone, et al. Navsim: Data-driven non-reactive autonomous vehicle simulation and benchmarking. *Advances in Neural Information Processing Systems*, 37:28706–28719, 2024.
- [90] Wei Cao, Marcel Hallgarten, Tianyu Li, Daniel Dauner, Xunjiang Gu, Caojun Wang, Yakov Miron, Marco Aiello, Hongyang Li, Igor Gilitschenski, et al. Pseudo-simulation for autonomous driving. *arXiv preprint arXiv:2506.04218*, 2025.
- [91] Xuefeng Jiang, Yuan Ma, Pengxiang Li, Leimeng Xu, Xin Wen, Kun Zhan, Zhongpu Xia, Peng Jia, Xianpeng Lang, and Sheng Sun. Transdiffuser: Diverse trajectory generation with decorrelated multi-modal representation for end-to-end autonomous driving. *arXiv preprint arXiv:2505.09315*, 2025.
- [92] Wenzhao Zheng, Ruiqi Song, Xianda Guo, Chenming Zhang, and Long Chen. Genad: Generative end-to-end autonomous driving. In *European Conference on Computer Vision*, pages 87–104. Springer, 2024.
- [93] Xiaolong Tang, Meina Kan, Shiguang Shan, and Xilin Chen. Plan-r1: Safe and feasible trajectory planning as language modeling. *arXiv preprint arXiv:2505.17659*, 2025.
- [94] Shuyao Shang, Yuntao Chen, Yuqi Wang, Yingyan Li, and Zhaoxiang Zhang. Drivedpo: Policy learning via safety dpo for end-to-end autonomous driving. *arXiv preprint arXiv:2509.17940*, 2025.